

Distribution Matching Variational AutoEncoder

Sen Ye^{1,3} Jianning Pei^{2,3} Mengde Xu³ Shuyang Gu^{3†}
 Chunyu Wang³ Liwei Wang¹ Han Hu³

¹ Peking University ² UCAS ³ Tencent

Abstract

*Most visual generative models compress images into a latent space before applying diffusion or autoregressive modelling. Yet, existing approaches such as VAEs and foundation model aligned encoders implicitly constrain the latent space without explicitly shaping its distribution, making it unclear which types of distributions are optimal for modeling. We introduce **Distribution-Matching VAE (DMVAE)**, which explicitly aligns the encoder’s latent distribution with an arbitrary reference distribution via a distribution matching constraint. This generalizes beyond the Gaussian prior of conventional VAEs, enabling alignment with distributions derived from self-supervised features, diffusion noise, or other prior distributions. With DMVAE, we can systematically investigate which latent distributions are more conducive to modeling, and we find that SSL-derived distributions provide an excellent balance between reconstruction fidelity and modeling efficiency, reaching gFID equals 3.2 on ImageNet with only 64 training epochs. Our results suggest that choosing a suitable latent distribution structure (achieved via distribution-level alignment), rather than relying on fixed priors, is key to bridging the gap between easy-to-model latents and high-fidelity image synthesis. Code is available at <https://github.com/senye/dmvae>.*

1. Introduction

The field of visual synthesis has made staggering progress, with generative models now capable of producing high-resolution, photorealistic images from complex text descriptions [25, 29]. A dominant paradigm underpinning these successes is a two-stage generation process [6, 28]. This approach first employs a powerful autoencoder, or “tokenizer,” to compress a high-dimensional image x into a compact, low-dimensional latent representation $z = E(x)$. Subsequently, a powerful generative model, such as a diffusion model [11, 31] or an autoregressive transformer [4, 24],

is trained to model the prior distribution $p(z)$ of these latents.

The primary motivation for this compression is twofold: it simplifies the data distribution, and it drastically reduces the computational complexity of modeling in the high-dimensional pixel space, thereby mitigating the curse of dimensionality. The efficacy of this entire pipeline, however, is critically dependent on the properties of the latent space \mathcal{Z} . An ideal latent distribution must be evaluated by two key criteria:

1. **Modeling Simplicity:** The aggregate latent distribution $q(z) = \int q(z|x)p(x)dx$ must be simple and well-structured, allowing the prior $q(z)$ to be learned easily and efficiently.
2. **Reconstruction Fidelity:** The latent code z must retain sufficient information to reconstruct the original image x perfectly via the decoder $G(z)$, maximizing $p(x|z)$.

Finding a distribution form that balances these two criteria is a key challenge in designing effective generative models.

Existing methods navigate this trade-off through various regularization strategies. The latent diffusion model [28], built upon a VAE framework, enforces a KL-constraint with a simple Gaussian, which simplifies modeling at the cost of information loss. VQ-VAE [33] and VQ-GAN [4] employ vector quantization, constraining the latent space to a finite, discrete codebook but introduces quantization artifacts. Recently, a promising alternative uses fixed self-supervised learning (SSL) features (e.g. DINO [2, 21]) as the latent space. While semantically rich and easy to model, these encoders [41] are fixed and were not trained for reconstruction, leading to a significant loss of fine-grained detail and poor reconstruction quality. To remedy this, SVG [30] adds learnable residual features, while VAAE [36] and AlignTok [3] train the autoencoder end-to-end but add an auxiliary loss to align the learned latents with the fixed DINO features. While this improves the balance, the final latent distribution is still the implicit result of two competing objectives (reconstruction and regularization), which limits our ability to explore the impact of different distribution forms on modeling effectiveness.

[†]Corresponding Author.

In this paper, we propose **Distribution Matching VAE (DMVAE)**, a novel generative framework that generalizes the VAE objective. DMVAE explicitly constrains the encoder’s aggregate posterior $q(z)$ to match an arbitrary, pre-defined reference distribution $p_r(z)$. This reference can be a Gaussian, a text-embedding distribution, or any empirically-defined distribution, such as the distribution of SSL features.

To achieve this, we leverage Distribution Matching Distillation (DMD) [38], a recent technique that aims to align two implicit distributions. DMD works by leveraging diffusion models as universal distribution estimators. It trains a diffusion model v_{real} on the reference distribution $p_r(z)$ to learn its score function $\nabla_z \log p_r(z, t)$. Our framework then trains the VAE by requiring that the score of its aggregate posterior, $q(z)$, matches this pre-computed reference score. This process effectively “distills” the structure of $p_r(z)$ onto $q(z)$, allowing us to mold the latent space into any desired shape, breaking free from the constraints of the Gaussian distribution.

DMVAE transforms the problem of autoencoder design into a problem of reference distribution selection. This allows us, for the first time, to systematically explore what kind of distribution is more conducive to modeling.

We conduct a large-scale study evaluating various reference distributions: (1) Gaussian distribution, (2) text-embedding (SigLIP [40]) distribution, (3) supervised learning (ImageNet classifier [7]) feature distribution, (4) self-supervised learning (DINO [2, 21]) feature distribution, and (5) noise distribution from intermediate diffusion [28] steps.

Our findings are decisive. We discover that different distribution forms have significantly different impacts on the difficulty of modeling and the quality of reconstruction. Our key finding is that SSL-derived features provide an excellent prior distribution—they are semantically structured enough to be trivial to model, yet sufficiently rich in information to permit high-fidelity reconstruction, demonstrating their superiority as a target distribution.

In summary, our contributions are:

1. We propose Distribution Matching VAE (DMVAE), a generalization of the VAE framework that can match the latent aggregate posterior to any pre-defined reference distribution.
2. We conduct the first large-scale, systematic study of various latent priors, systematically evaluating the pros and cons of different latent priors (e.g., SSL feature distributions) as modeling targets.
3. Using DMVAE as a tokenizer with an SSL prior, our model achieves a state-of-the-art gFID of 3.22 on ImageNet 256x256 with only 64 training epochs and a gFID of 1.82 with 400 training epochs, demonstrating the profound impact of optimizing the latent prior.

2. Preliminary

We first define the notation used throughout the paper. Let $x \in \mathcal{X}$ be an input image from the data distribution $p(x)$. A tokenizer consists of an encoder $E : \mathcal{X} \rightarrow \mathcal{Z}$ that maps the image to a latent code $z = E(x)$, and a decoder $G : \mathcal{Z} \rightarrow \mathcal{X}$ that reconstructs the image $\hat{x} = G(z)$. The core problem is to design E and G such that z is both informative (low reconstruction error) and easy to model (simple aggregate posterior $q(z) = \int q(z|x)p(x)dx$).

2.1. Variational Autoencoders (VAEs)

The standard β -VAE [13] framework trains the encoder E (which parameterizes $q(z|x)$) and decoder G (which parameterizes $p(x|z)$) by optimizing the Evidence Lower Bound (ELBO):

$$\mathcal{L}_{\text{VAE}} = \mathbb{E}_{x \sim p(x)} [\mathbb{E}_{q(z|x)} [\log p(x|z)] - \beta D_{KL}(q(z|x) || p(z))] \quad (1)$$

where $p(z)$ is a fixed, simple prior, typically a standard Gaussian $N(0, I)$. The KL-divergence term acts as a regularizer, forcing the per-sample posterior $q(z|x)$ to be close to $p(z)$, which in turn simplifies the aggregate posterior $q(z)$.

While a large β was initially intended for strong regularization to ensure generative capacity, it frequently causes model collapse. Consequently, in latent diffusion models which use VAE as tokenizer, β is often set to a very small value (e.g., $1 \times e^{-6}$ in [28]).

2.2. Inject distribution prior into VAEs

Recent works have explored moving beyond a simple Gaussian prior.

VAAE [3, 36] proposes to explicitly align the latent codes $z = E(x)$ with the features from a pre-trained DINO model, denoted as $\phi(x)$. This is implemented as an auxiliary pairwise similarity loss, balancing reconstruction with alignment:

$$\mathcal{L}_{\text{VAAE}} = \mathcal{L}_{\text{Recon}} + \lambda D_{\text{pair}}(E(x) - \text{sg}[\phi(x)])^2 \quad (2)$$

where $\text{sg}[\cdot]$ denotes a stop-gradient operator. This encourages $E(x)$ to inherit the semantic properties of $\phi(x)$. Conceptually, setting λ to an extremely large value can be seen as freezing the DINO model and using it directly as the encoder [41].

Diffusion Priors [17] attempts to directly use a pre-trained diffusion model as the prior $p(z)$. The score of this powerful prior, $\nabla_z \log p(z)$, is used to optimize the encoder by maximizing the likelihood of the encoder’s output under $p(z)$:

$$\mathcal{L}_{\text{flowprior}} = \mathbb{E}_{t, x \sim p(x), \epsilon \sim \mathcal{N}(0, I)} [||v_{\theta}(E(x), t) - (\epsilon - E(x))||^2] \quad (3)$$

While flexible, directly backpropagating the diffusion loss through the encoder is notoriously unstable and can lead to posterior collapse[22].

Adversarial Autoencoders (AAE) [20] uses a GAN-based objective to shape the latent distribution. An auxiliary discriminator D is trained to distinguish between samples from the aggregate posterior $q(z)$ and a reference prior $p_r(z)$. The encoder E is simultaneously trained as a generator to fool D :

$$\begin{aligned} \mathcal{L}_{\text{AAE}} = & \mathcal{L}_{\text{Recon}} + \\ \min_E \max_D & \mathbb{E}_{z \sim p_r(z)} [\log D(z)] + \mathbb{E}_{x \sim p(x)} [\log(1 - D(E(x)))] \end{aligned} \quad (4)$$

This allows $q(z)$ to match $p_r(z)$. However, AAEs are limited by the instability of GAN training and the expressive capacity of D , which has practically restricted $p_r(z)$ to simple distributions like Gaussian mixtures. Our work aims to overcome this limitation by utilizing diffusion, which allows $p_r(z)$ to be more complex distributions.

3. Distribution Matching VAE

The Pitfall of Per-Sample Regularization. Our goal is to solve the ‘‘Tokenizer’s Dilemma’’ by gaining explicit control over the aggregate posterior distribution $q(z) = \int q(z|x)p(x)dx$. Previous methods [3, 36] attempt this indirectly via per-sample regularization, which is fundamentally insufficient. The classic VAE loss (Eq. (1)) regularizes the per-sample posterior $q(z|x)$. While this forces each $q(z|x)$ towards the prior $p(z)$, it places no explicit constraint on the mixture of these posteriors, $q(z)$. If the decoder is powerful, the encoder can learn to map different inputs x to distinct, well-separated modes, (i.e., $q(z|x)$ collapses to a delta function). The resulting aggregate posterior $q(z)$ becomes a complex, multi-modal, and ‘‘holey’’ manifold [26, 27], which is notoriously difficult for a generative prior $p(z)$ to model. Similarly, methods like VAVAE [3] (Eq. (2)) use a per-sample distance loss, which only guarantees that each $E(x)$ is near its corresponding $\phi(x)$, but does not constrain the global structure of the $q(z)$ manifold.

Score-Based Distribution Matching. To overcome this, we must impose a constraint directly on the aggregate distribution $q(z)$. We propose the **Distribution Matching VAE (DMVAE)**, which forces $q(z)$ to match an arbitrary, pre-defined reference distribution $p_r(z)$.

The challenge is that both $q(z)$ (from the encoder) and $p_r(z)$ (e.g., SSL features) are complex, implicit distributions. We cannot tractably compute $D_{KL}(q(z)||p_r(z))$. While an adversarial loss (Eq. (4)) is one option, it is unstable and expressively limited.

Instead, we turn to diffusion models. A key insight is that any distribution $p(z)$ is uniquely characterized by its time-dependent score function $\nabla_z \log p_t(z_t)$ [31]. Therefore, we can utilize diffusion model as a universal distribution estimator and compute the gradient of $D_{KL}(q(z)||p_r(z))$ through their score functions, following the approach in [38]

3.1. The DMVAE Objective.

Our method does not pre-compute and distill a fixed score, as this fails when the student distribution (our $q(z)$) is constantly changing. Instead, we follow the joint-training mechanism of Distribution Matching Distillation [38].

Our framework involves a ‘‘real’’ (teacher) score model $s_{\text{real}}(\cdot, \cdot)$ and a ‘‘fake’’ (student) score model $s_{\text{fake}}(\cdot, \cdot)$, trained alongside the VAE (E_θ, G_ω).

Step 1: Pre-train Reference Score Model (Teacher).

First, we train a time-conditioned velocity network $v_{\text{real}}(\cdot, \cdot)$ on the fixed reference distribution $p_r(z)$ using the flow matching objective [18]:

$$\mathcal{L} = \mathbb{E}_{t, z_0 \sim p_r(z), \epsilon \sim N(0, I)} [||v_{\text{real}}(\alpha_t z_0 + \sigma_t \epsilon, t) - (\epsilon - z_0)||_2^2] \quad (5)$$

Once trained, v_{real} is frozen and serves as the canonical representation of our reference distribution. The score $s_{\text{real}}(z_t, t) = \nabla \log p_{r,t}(z_t)$ can be obtained by a linear transformation of velocity v_{real} using SDE formulations [19].

Step 2: Joint Training of VAE and Fake Score Model (Student). We then jointly train the VAE (E_θ, G_ω) and the fake score model s_{fake} . The fake model’s job is to learn the score function of the encoder’s aggregate posterior $q(z)$, even as $q(z)$ changes during training. The VAE is, in turn, trained to change its output $z = E(x)$ so that the aggregated posterior $q(z)$ matches with reference distribution $p_r(z)$.

This results in a total objective with three components:

$$\mathcal{L}_{\text{Total}} = \mathcal{L}_{\text{recon}}(E_\theta, G_\omega) + \gamma \mathcal{L}_{\text{fm}}(E_\theta, s_{\phi_q}) + \lambda \mathcal{L}_{\text{DM}}(E_\theta, s_{\phi_q}) \quad (6)$$

Reconstruction Loss (Trains E_θ, G_ω): we follow [28, 36] to leverage a standard perceptual loss and a GAN loss to ensure fidelity:

$$\mathcal{L}_{\text{recon}} = \mathbb{E}_{x \sim p(x)} [d(x, G_\omega(E_\theta(x)))] \quad (7)$$

Fake Score Model Loss (Trains s_{fake}): This loss trains s_{fake} to capture the score function for the current $q(z)$. We stop the gradient of E_θ so that this loss only updates v_{fake} . In practice implementation, we adopt flow matching objective to learn v_{fake} and convert it to s_{fake} :

$$\mathcal{L}_{\text{fm}} = \mathbb{E}_{t, x \sim p(x), \epsilon} [||v_{\text{fake}}(\alpha_t z_0 + \sigma_t \epsilon, t) - (\epsilon - z_0)||_2^2] \quad (8)$$

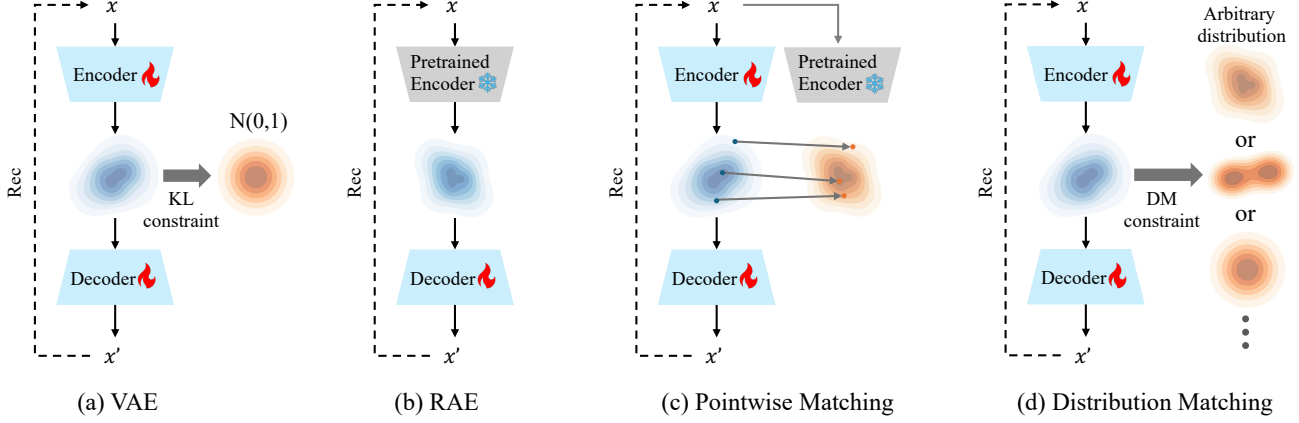


Figure 1. Illustration of VAE [13], RAE [41], pointwise matching encoder [3, 36], and Distribution Matching VAE.

where z_0 is $\text{StopGradient}[E_\theta(x)]$.

Distribution Matching Loss (Trains E_θ): It penalizes the encoder E_θ by comparing the scores of the student and teacher models. Following [38], we compute the gradient directly without back-propagating through the fake score network:

$$\nabla_\theta \mathcal{L}_{\text{DM}} \simeq \mathbb{E}_{t,x} [w_t(s_{\text{fake}}(z_t, t) - s_{\text{real}}(z_t, t)) \frac{dE_\theta(x)}{d\theta}] \quad (9)$$

where $z_t = \alpha_t E_\theta(x) + \sigma_t \epsilon$. w_t are weighting functions to balance different noise levels following [38]. By default, t is sampled uniformly from $[0, 1]$.

In summary, this joint training creates a dynamic where \mathcal{L}_{fm} forces s_{fake} to track the score of the aggregate posterior $q(z)$, and \mathcal{L}_{DM} pushes E_θ to ensure $q(z)$ structurally aligns with $p_r(z)$.

Step 3: Decoder refinement. After the joint training converges, we can optionally perform decoder refinement. Following [3], we freeze the encoder and finetune the decoder for a few iterations using only the reconstruction loss. This step allows the decoder to fully adapt to the latent manifold, which can yield a slight improvement in final reconstruction fidelity.

Per-Sample vs. Distributional Constraints. The distribution matching formulation (Eq. (6)) is fundamentally different from VAEs (Eq. (1)) or VAAE (Eq. (2)). The key difference lies in how they behave under the inevitable tension between the reconstruction loss $\mathcal{L}_{\text{Recon}}$ and the prior constraint.

Per-sample losses, such as the VAE’s KL-divergence or VAAE’s pairwise distance, optimize an *expectation* of a local loss: $\mathbb{E}_x[\mathcal{L}(E_\theta(x), \dots)]$. This objective can be deceptively minimized. Consider a special case: For half the data $\{x_A\}$, $\mathcal{L}_{\text{Recon}}$ dominates and $\mathcal{L}_{\text{align}}$ dominates the other

half $\{x_B\}$. Under the joint optimization, suppose the latents $E_\theta(x_A)$ remain on the original reconstruction manifold $\mathcal{M}_{\text{recon}}$, and $E_\theta(x_B)$ are pulled perfectly onto the prior $p_r(z)$. In this case, the *total average alignment loss* $\mathbb{E}[\mathcal{L}_{\text{align}}]$ is halved. However, the aggregate posterior $q(z)$ has *degenerated* into a disjoint mixture $q(z) \approx 0.5 \cdot \mathcal{M}_{\text{recon}} + 0.5 \cdot p_r(z)$. This topologically damaged manifold is arguably *worse* for generative modeling than the original $\mathcal{M}_{\text{recon}}$, despite the seemingly low average aligned loss.

In contrast, our DMVAE objective optimizes a *global geometric divergence* $D_{\text{KL}}(q(z)||p_r(z))$. This loss cannot be deceptively minimized in this way. The score function $\nabla \log q(z)$ of the disjoint mixture distribution described above is globally different from the (presumably smoother) score $\nabla \log p_r(z)$ of the target prior. Therefore, s_{fake} (which must track this complex score) will fail to match s_{real} , causing the distribution matching loss to remain high. Even if $\mathcal{L}_{\text{Recon}}$ prevents a perfect match, \mathcal{L}_{DM} will always push $q(z)$ towards a holistic structural alignment with $p_r(z)$, resulting in a denser, non-hole manifold that is far more suitable for a generative prior.

Matching the Dimensionality of Distributions. In practice, the latent dimension of our encoder $E_\theta : \mathcal{X} \rightarrow \mathbb{R}^{d_e}$ may not match the reference distribution $p_r(z)$ (where $z \in \mathbb{R}^{d_r}$). To resolve this, we introduce a light-weight, learnable projection head $H_\phi : \mathbb{R}^{d_e} \rightarrow \mathbb{R}^{d_r}$. Specially, for projection to spatially aligned reference distribution, the head is a two-layer MLPs and otherwise, the head is a two-layer transformer decoder with learnable queries [1].

As depicted in Fig. 2, the data flow is as follows: The encoder produces a latent code $z_e = E_\theta(x)$. This z_e is used by the decoder for reconstruction, $G_\omega(z_e)$. Concurrently, z_e is passed through the projector to get $z_0 = H_\phi(z_e)$, and z_t is obtained by adding noise to it will be used in the \mathcal{L}_{DM} loss (Eq. (9)). The gradient flow is crucial:

- The decoder G_ω is optimized only by $\mathcal{L}_{\text{Recon}}$.

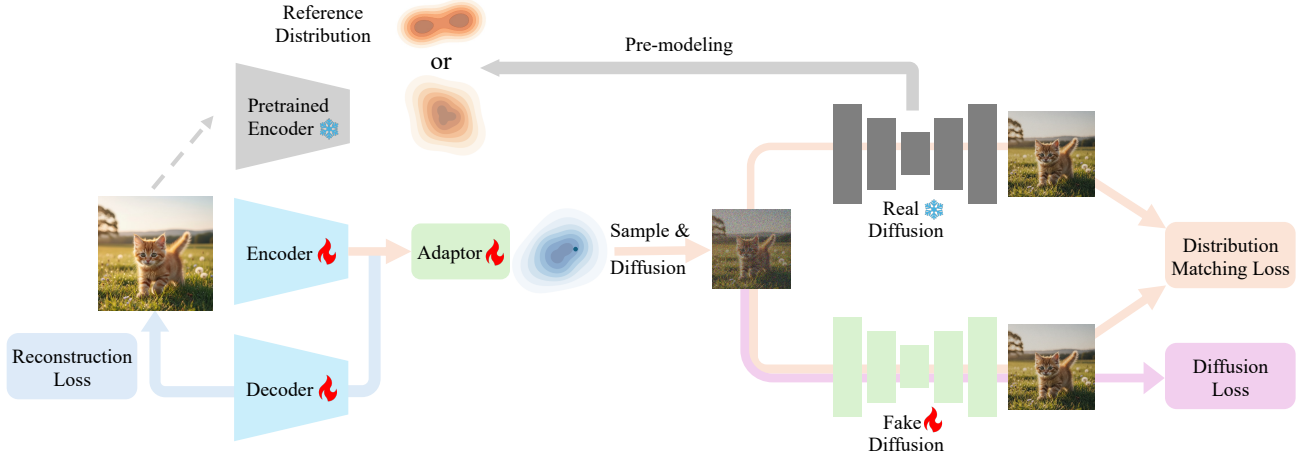


Figure 2. The training pipeline of Distribution Matching VAE.

- The projection head H_ϕ is optimized only by \mathcal{L}_{DM} .
- The encoder E_θ is optimized by both $\mathcal{L}_{\text{Recon}}$ and \mathcal{L}_{DM} .
- The diffusion loss is only used to update the fake diffusion model (v_{fake}).

This architecture forces E_θ to learn a representation z_e that is simultaneously optimal for reconstruction and matches the structure of the reference distribution $p_r(z)$.

3.2. Stabilizing the Distant Distribution Matching.

We empirically found that the joint-training objective (Eq. (6)) can be unstable when the aggregate posterior $q(z)$ is far from the reference $p_r(z)$. This stems from a fundamental dilemma in score matching [31, 38].

- On one hand, using a **large noise scale** σ_t ensures support overlap, but this level of smoothing “washes out” the fine-grained, high-frequency differences between the distributions, leading to a flat loss landscape for \mathcal{L}_{DM} and causing vanishing gradients.
- On the other hand, a **small noise scale** σ_t preserves distribution details but, when $q(z)$ and $p_r(z)$ is distant, it suffers from disjoint supports. This causes high-variance, explosive gradients that destabilize the entire joint-training process and can lead to mode collapse.

Crucially, unlike prior works [12, 38] leveraging distribution matching for distillation—where an implicit pairing or regression loss keeps the distributions proximate—our framework is, to our knowledge, the first to use this mechanism to match the entire aggregate posterior $q(z)$ of an autoencoder to an unpaired reference $p_r(z)$. The potentially vast initial discrepancy $D(q(z)||p_r(z))$ makes the system highly susceptible to the aforementioned instabilities.

To effectively mitigate these inherent training difficulties and ensure convergence, we adopt several stabilizing training strategies: we utilize the pretrained weights of the real score model to initialize the fake score model and train the VAE from a pretrained encoder, providing a stable start-

ing point; implement alternating training between the VAE and the fake score model to balance the learning dynamics [38]. Furthermore, we reduce all latent spaces and priors to a low dimension (e.g., $d = 32$) with reconstruction objective. This step is critical as it helps mitigate the curse of dimensionality, thus reducing the sparsity and computational challenges associated with distribution matching in high-dimensional spaces.

3.3. Variations of Distribution Matching Objective

To investigate the optimal objective for aligning the aggregate posterior $q(z)$ with the reference prior $p_r(z)$, we analyze several distinct gradient fields derived from different score-based objectives. We visualize the learned latent distribution in a 2D toy experiment by these objectives, as shown in Figure 3, and mathematically analyze their gradients to understand their convergence behaviors. For brevity, we omit time-dependent weights w_t and the chain rule term $\frac{dE_\theta(x)}{d\theta}$, focusing on the gradient field $\nabla_z \mathcal{L}$ that acts on the latent samples $z = E_\theta(x)$.

Real Score Maximization. This objective also referred to as a “Flow Prior” [17], maximizes the likelihood of the encoder’s output under a fixed, pre-trained reference teacher model s_{real} . This corresponds to minimize real model’s flow matching loss. Depending on the stop-gradient placement, we identify three variations, illustrated in Figure 3 (d, e, f). As the gradient update pushes latent codes z solely towards high-density regions of $p_r(z)$, this objective lacks a mechanism to encourage entropy or coverage. Consequently, it suffers from **mode dropping**, where the latent distribution collapses into a few modes rather than covering the entire manifold.

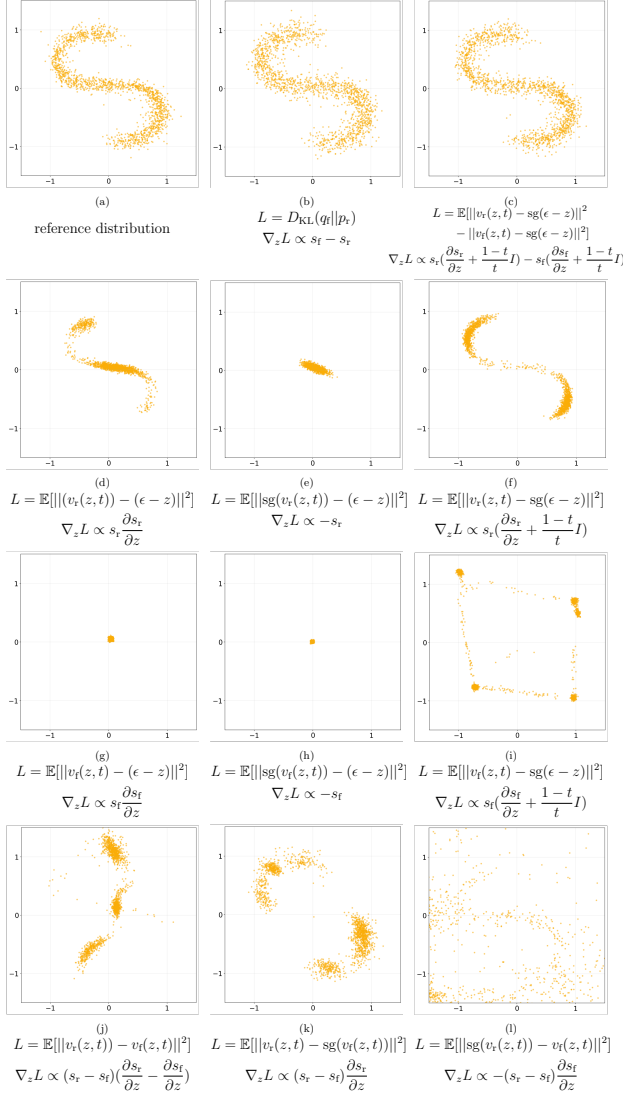


Figure 3. Analysis of different distribution matching objectives on a 2D setting. (a) illustrates the reference distribution; (b) denotes the distribution matching objective, (d,e,f) represent real score maximization with different stopping gradients; (g,h,i) represent methods for fake score maximization; (j,k,l) represent directly optimizing the difference between real and fake scores; Finally, (c) represents optimizing the difference between the real and fake diffusion losses. For each objective, we have listed the loss function and their gradient $\nabla_z \mathcal{L}$.

Fake Score Maximization (End-to-End). This approach jointly trains the encoder and the diffusion model (student s_{fake}) without an explicit reference anchor. It aims to minimize the denoising error of the student model on its own generated samples. Similar to the failure mode discussed in REPA-E [15], this creates a self-reinforcing loop leads to mode collapse, which is more severe than real score maximization. As shown in Figure 3 (g, h, i), the trivial solution

for minimizing this objective is for the latent space to contract to a single or a few points, which is trivially easy to model but useless for generation.

Score Differences minimization. An intuitive idea is to minimize the L_2 distance between score functions $\|s_{\text{fake}}(z) - s_{\text{real}}(z)\|^2$ thereby optimizing the input distribution. While theoretically sound, our experiments show that optimization is unstable, failing to align the distributions effectively as shown in Figure 3 (j, k, l).

Loss Differences minimization. This objective minimizes the difference in flow matching losses: $\mathcal{L} = \|v_{\text{real}} - \text{sg}(\epsilon - z)\|^2 - \|v_{\text{fake}} - \text{sg}(\epsilon - z)\|^2$. While it successfully aligns the distribution, the gradient computation involves the *Jacobian* of the score network, which is computationally expensive and memory-intensive for high-dimensional image latent spaces.

Ours: Distribution Matching objective. The distribution matching objective overcomes the aforementioned limitations—mode collapse, mode dropping, and computational inefficiency. The gradient is approximated as the difference between score functions: $\nabla_z \mathcal{L}_{\text{DM}} \propto s_{\text{fake}}(z) - s_{\text{real}}(z)$. Crucially, this objective constructs a *difference vector field* that pulls them towards the high-density modes of $p_r(z)$ (via $+s_{\text{real}}$) and avoids mode collapse to a single mode through $-s_{\text{fake}}$. As illustrated in Figure 3 (b), this balanced dynamic achieves precise distribution alignment that preserves the global structure of the reference without the Jacobian overhead.

4. Selection of Reference Distributions

A key advantage of DMVAE is its ability to flexibly incorporate *any* distribution as the latent prior $p_r(z)$. This allows us, for the first time, to systematically investigate the “Tokenizer’s Dilemma”: what choice of $p_r(z)$ yields the best balance of reconstruction fidelity and modeling simplicity?

We conduct our primary investigation on the ImageNet 256x256 dataset. We categorize our candidate reference distributions into two families:

Category 1: Data-Derived Distributions. These priors are derived directly from the ImageNet training data, and are therefore semantically aligned with the data manifold.

- **SSL Features:** The aggregate posterior of a pre-trained DINOv2-ViT/L [21] model.
- **Supervised Features:** The aggregate posterior of a supervised ResNet-34 [7] classifier.
- **Text Features:** We generate captions for ImageNet and extract features using a pre-trained SigLIP [40] text encoder.

Table 1. Variations for different reference distributions.

Ref distribution	rFID ↓	PSNR ↑	gFID-5k ↓
VAE-baseline	0.54	25.7	27.3
DINO	0.81	21.8	13.1
Resnet	1.46	20.9	18.6
SigLIP-text	1.63	24.0	26.8
Difftraj	0.60	26.9	31.8
SubDino	0.29	25.6	37.9
GMM	0.42	27.3	29.6
Gaussian	0.47	27.4	26.6

- **Diffusion Noise States:** The aggregate distribution of noisy latents z_t (at $t = 0.5$) from a pre-trained LDM [28] on ImageNet.

Category 2: Data-Independent Distributions. These priors are either synthetic or are not representative of the full data distribution.

- **Sub-sampled SSL features:** DINO features extracted from only 10 classes of ImageNet, creating a multi-modal distribution simpler than the full prior.
- **Standard Gaussian:** A simple $\mathcal{N}(0, I)$, as used in classic VAEs.
- **Gaussian Mixture Model (GMM):** A 10-component GMM, representing a simple, multi-modal synthetic baseline.

Experimental Setting. A fair comparison is challenging, as the difficulty of matching $q(z)$ to $p_r(z)$ depends on the distance and structural similarity between $p_r(z)$ and the original data manifold. As a preliminary setting for this exploration, we adopt a heuristic-based weighting. For data-derived priors, which are presumably closer to the original data, we set a higher matching weight of $\lambda_{DM} = 10$. For synthetic priors, we set $\lambda_{DM} = 1$. All other loss weights are held constant. All models are trained for 300k iterations with batch size 256.

The results, summarized in Tab. 1, show that the self-supervised DINO features provide the best overall balance of reconstruction quality and generative modeling performance.

t-SNE Visualization and Analysis. To understand *why* the SSL prior yields superior results, we performed a t-SNE visualization. We randomly sampled 100 images from 20 distinct ImageNet classes. We then visualized the reference distribution $p_r(z)$ and the latents $q(z)$ from our DMVAE trained to match reference distribution. The results are shown in Fig. 4.

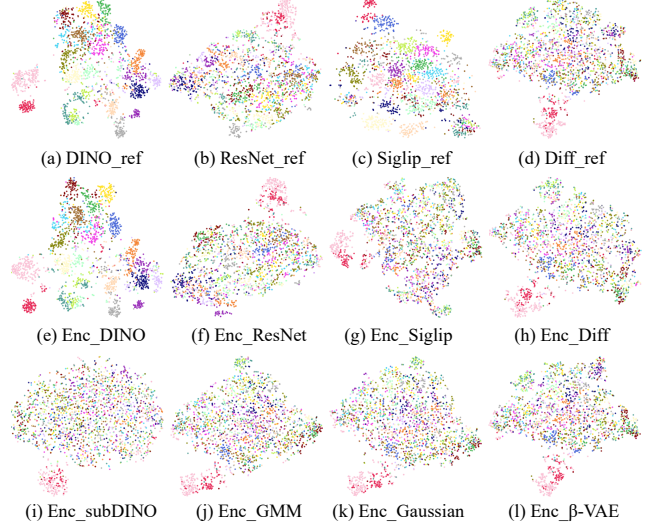


Figure 4. Illustration of t-SNE on different distributions. (a-d) represent four different reference distributions, (e-h) represent the distribution of the DMVAE encoder learned from these four reference distributions, (i-k) represent the encoder distribution learned from the data-independent distribution, and (l) represents the distribution of the β -VAE encoder output.

The visualization clearly shows that the original DINO features (Fig. 4 a) possess superior semantic clustering. This inherent semantic organization likely reduces the complexity for the subsequent diffusion modelling, as it can focus on modeling intra-class variations rather than struggling with semantic confusion. Furthermore, the DMVAE latents (Fig. 4 e) successfully replicate this strong clustering structure, demonstrating that the distribution matching constraint effectively enforces the global geometry of the reference prior. In contrast, the β -VAE latents (Fig. 4 l) or DMVAE constrained by data-independent distributions demonstrated in the last row, struggles on distinguish different semantic modes. This confirms a more structured and semantically meaningful latent space is crucial for efficient generation.

5. Experiments

To investigate the effectiveness of DMVAE, we conducted all experiments using the common ImageNet-256 setting. We first trained the DMVAE model on the ImageNet training set and evaluated its reconstruction quality on the validation set using PSNR and rFID. To measure the modeling difficulty of the acquired latent representation, we then trained a Lightning-DiT [36] diffusion model and measured its generative quality using gFID. By default, the reported generation results do not employ guidance strategies such as Classifier-free Guidance [10].

Table 2. Ablation studies on diffusion matching weight, network size, CFG weight and timestep schedule.

Factor	Setting	PSNR ↓	rFID ↓	gFID-5k ↓
Default	($\lambda = 10$, L-Net, CFG=1.0, Uniform)	22.1	0.44	13.1
DM Weight	$\lambda_{DM} = 1$	25.2	0.37	16.7
	$\lambda_{DM} = 20$	21.4	0.78	12.5
	$\lambda_{DM} = 100$	19.6	0.82	12.6
Score Net Size	Small	22.9	0.67	13.9
	XL	21.7	0.91	12.5
CFG Weight	3.0	20.6	1.02	11.6
	5.0	19.4	1.26	11.5
Timestep Schedule	[0,1] annealing to [0,0.5]	21.9	0.55	12.7

Table 3. Class-conditional generation results on ImageNet 256×256 .

Method	Reconstruction		Training Epochs	#Params	Generation	
	PSNR↑	rFID↓			gFID↓	IS↑
AutoRegressive (AR)						
LlamaGen [32]	24.45	0.59	300	3.1B	9.38	112.9
MAR [16]	24.08	0.87	800	945M	2.35	227.8
Latent Diffusion Models						
SiT [19]	26.0	0.61	1400	675M	8.61	131.7
FasterDit [35]	26.0	0.61	400	675M	7.91	131.3
RAE(DiT ^{DH} -XL) [41]	18.9	0.57	800	839M	1.51	242.9
RAE(DiT-XL) [41]	18.9	0.57	800	675M	1.87	209.7
VA-VAE [36]	27.6	0.28	64	675M	5.14	130.2
VA-VAE [36]	27.6	0.28	800	675M	2.17	205.6
AlignTok [3]	25.8	0.26	64	675M	3.71	148.9
AlignTok [3]	25.8	0.26	800	675M	2.04	206.2
DMVAE	21.5	0.64	64	675M	3.22	171.7
DMVAE	21.5	0.64	400	675M	1.82	206.9
DMVAE	21.5	0.64	800	675M	1.64	216.3

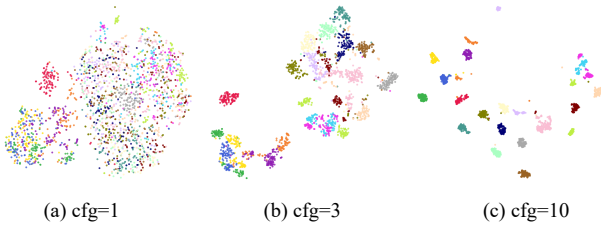


Figure 5. Different CFG scale represents different distributions.

5.1. Ablation Studies

Many factors influence the training of our tokenizer. We ablate the most critical hyperparameters, starting from a default configuration: we adopt DINO to provide reference distributions, $\lambda_{DM} = 10$, and use “Lightning-DiT-L” for both real and fake score network, and timestep is uniformly

sampled from $[0, 1]$. Besides, we do not adopt CFG [10] for both real and fake diffusion models and the evaluation. Each tokenizer is trained for 250K iterations and we use a DiT-L model trained with 300K iterations with batch size of 256. We vary each factor independently, with results reported in Tab. 2.

- **DM Weight (λ_{DM}):** A weight of 10 provides the best balance. A lower weight (e.g., 1) results in poor generative quality due to weak regularization. Conversely, a higher weight (e.g., 100) strengthens the generative prior but degrades reconstruction performance by enforcing an overly strict constraint.
- **Score Network Size:** We observe that a larger score network, which can more accurately model the reference and latent distribution, leads to improved distribution match-

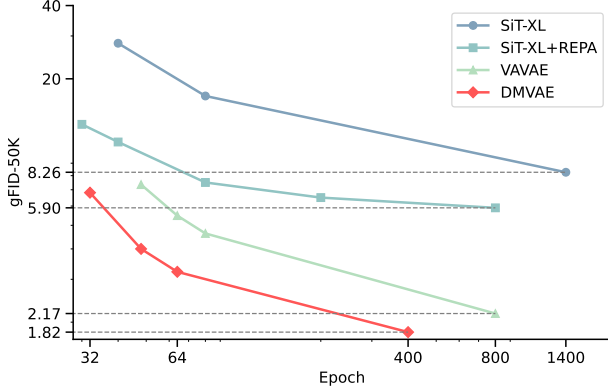


Figure 6. Comparison of the convergence speed.

ing and better final generative quality.

- **Classifier-Free Guidance (CFG):** While our default setting disables CFG (guidance weight of 1.0), we find that applying a small CFG weight (e.g., 3.0) during the score matching process (Eq. (9)) can slightly improve generative quality, albeit at a minor cost to reconstruction. We visualize how the real diffusion models the reference distribution under different CFG weights in Fig. 5. We find that a suitable CFG brings a stronger semantic clustering properties, which can better accelerate convergence. When CFG scale is extremely large, the distribution may be disjoint that makes training unstable.
- **Timestep schedule:** We compare our default uniform sampling ($t \sim U[0, 1]$) with a noise schedule annealing strategy. Following [34], the annealing setting starts at $[0, 1]$ and linearly contracts the sampling range to $[0, 0.5]$. We find that annealing provides a slight improvement by focusing on more precise, low-noise matching in the later stages of training.

5.2. Comparison with other methods

Finally, we compare our DMVAE tokenizer against other state-of-the-art tokenizer methods. We generate 50000 samples through 250 sampling steps without CFG. We show the results in Tab. 3. DMVAE outperforms all the competing methods. With merely 400 training epochs, DMVAE surpasses the performance of the state-of-the-art methods, including RAE(DiT-XL) and AlignTok, achieving a 2× improvement in training efficiency. Besides, we also plot the generation quality of diffusion model in the training process in Fig. 8. DMVAE enables significantly faster convergence than baseline methods.

6. Related Work

Visual Tokenizers Visual Tokenizers aim to compress high-dimensional image data into a compact latent representation, a strategy that has become fundamental to modern visual generative models (the “compress then model”

paradigm). [33] pioneered this by introducing a Vector-Quantized Variational Autoencoder, which enabled autoregressive modeling in a discrete latent space, successfully moving beyond direct pixel-space operations. Building on this, VQGAN [4] further improved performance by integrating an adversarial loss into the VAE training objective, which significantly enhanced the perceptual quality and synthesis of fine details in reconstructed images. Concurrently, Latent Diffusion Models [28] adapted this paradigm by training a VAE [13] with a modest KL regularization, and subsequently modeling the resulting continuous latent distribution using a diffusion process. Recently, researches [36, 39] has highlighted the reconstruction-generation dilemma, noting that improved reconstruction quality does not always correlate with superior generative performance, suggesting a potential trade-off [36]. This observation has spurred research into alternative regularization methods. To mitigate this, approaches like VA-VAE [36] and AlignTok [3] propose aligning the VAE’s latent representations with the semantic features extracted from powerful, pre-trained Vision Foundation Models (VFMs) [8, 21, 23, 40]. Furthermore, RAE [41] explored using a frozen VFM as the encoder, training only a corresponding decoder for reconstruction. However, this strategy often results in poor reconstruction quality, suffering from a significant loss of fine-grained visual details. While these VFM-based methods initially explored semantic regularization, they all rely on point-wise alignment (e.g., minimizing distance between individual latent vectors and VFM features). Unlike these methods, we expand the concept of regularization to distribution matching and directly shape the entire latent distribution to a desired prior, leading to a more globally consistent and generative-friendly latent space.

Distribution Matching Distribution matching is a long-standing problem in generative modeling, focusing on finding a transformation or mapping (transport) between different probability distributions. Variational Autoencoders (VAEs) [9, 13] apply this by aiming to match the encoded hidden states of images to a simple Gaussian distribution, which then enables image generation from randomly sampled Gaussian vectors. Adversarial Autoencoders (AAE) [20] addressed the common mode collapse issue [26, 27] of VAEs by introducing adversarial learning [5] to enforce the alignment of the image latent distribution with an arbitrary prior. However, AAE struggles to match complex target distributions due to the limited capacity of the standard discriminator. The most related technique to our work is the Variational Score Matching [34] used in diffusion model distillation [34, 37, 38, 42]. This technique successfully distills a student generative model from a teacher by directly comparing and aligning their re-

spective score functions. We adopt this distribution matching technique, but apply it to match the hidden representations of visual tokenizers with a predefined prior distribution. This distribution-level regularization allows us to shape a better-structured and more generative latent space for subsequent image modeling.

7. Conclusion and Limitation

In this work, we introduced the Distribution Matching VAE (DMVAE), a framework that, for the first time, allows the aggregate posterior of an autoencoder to be constrained at the *distributional level*. This enabled us to systematically explore the core question of “what kind of latent distribution is more beneficial for modeling.” Our key finding is that using semantically-rich, self-supervised features like DINO as a reference distribution performs excellently in terms of both reconstruction fidelity and generative tractability, proving the superiority of this type of distribution. This approach is highly efficient, achieving an excellent gFID of 3.22 on ImageNet after only 64 epochs of training. We believe DMVAE offers a significant advancement for all two-stage generative models and can be broadly applied to tasks in audio, video, and 3D generation.

While our method is powerful, we acknowledge that matching distributions that are initially far apart remains a challenge, often requiring careful tuning. This makes the reference distribution more like a regularizer than a complete matching, which limits our precise control over the tokenizer’s output distribution. In the future, we would focus on developing more robust optimization techniques for this distant-matching problem. Solving this will fully unlock the potential of designing generative latent spaces.

References

- [1] Nicolas Carion, Francisco Massa, Gabriel Synnaeve, Nicolas Usunier, Alexander Kirillov, and Sergey Zagoruyko. End-to-end object detection with transformers. In *European conference on computer vision*, pages 213–229. Springer, 2020. 4
- [2] Mathilde Caron, Hugo Touvron, Ishan Misra, Hervé Jégou, Julien Mairal, Piotr Bojanowski, and Armand Joulin. Emerging properties in self-supervised vision transformers. In *Proceedings of the IEEE/CVF international conference on computer vision*, pages 9650–9660, 2021. 1, 2
- [3] Bowei Chen, Sai Bi, Hao Tan, He Zhang, Tianyuan Zhang, Zhengqi Li, Yuanjun Xiong, Jianming Zhang, and Kai Zhang. Aligning visual foundation encoders to tokenizers for diffusion models. *arXiv preprint arXiv:2509.25162*, 2025. 1, 2, 3, 4, 8, 9, 12
- [4] Patrick Esser, Robin Rombach, and Bjorn Ommer. Taming transformers for high-resolution image synthesis. In *Proceedings of the IEEE/CVF conference on computer vision and pattern recognition*, pages 12873–12883, 2021. 1, 9, 12
- [5] Ian Goodfellow, Jean Pouget-Abadie, Mehdi Mirza, Bing Xu, David Warde-Farley, Sherjil Ozair, Aaron Courville, and Yoshua Bengio. Generative adversarial networks. *Communications of the ACM*, 63(11):139–144, 2020. 9
- [6] Shuyang Gu, Dong Chen, Jianmin Bao, Fang Wen, Bo Zhang, Dongdong Chen, Lu Yuan, and Baining Guo. Vector quantized diffusion model for text-to-image synthesis. In *Proceedings of the IEEE/CVF conference on computer vision and pattern recognition*, pages 10696–10706, 2022. 1
- [7] Kaiming He, Xiangyu Zhang, Shaoqing Ren, and Jian Sun. Deep residual learning for image recognition. In *Proceedings of the IEEE conference on computer vision and pattern recognition*, pages 770–778, 2016. 2, 6
- [8] Kaiming He, Xinlei Chen, Saining Xie, Yanghao Li, Piotr Dollár, and Ross Girshick. Masked autoencoders are scalable vision learners. In *Proceedings of the IEEE/CVF conference on computer vision and pattern recognition*, pages 16000–16009, 2022. 9
- [9] Irina Higgins, Loic Matthey, Arka Pal, Christopher Burgess, Xavier Glorot, Matthew Botvinick, Shakir Mohamed, and Alexander Lerchner. beta-vae: Learning basic visual concepts with a constrained variational framework. In *International conference on learning representations*, 2017. 9
- [10] Jonathan Ho and Tim Salimans. Classifier-free diffusion guidance. *arXiv preprint arXiv:2207.12598*, 2022. 7, 8
- [11] Jonathan Ho, Ajay Jain, and Pieter Abbeel. Denoising diffusion probabilistic models. *Advances in neural information processing systems*, 33:6840–6851, 2020. 1
- [12] Xun Huang, Zhengqi Li, Guande He, Mingyuan Zhou, and Eli Shechtman. Self forcing: Bridging the train-test gap in autoregressive video diffusion. *arXiv preprint arXiv:2506.08009*, 2025. 5
- [13] Diederik P Kingma and Max Welling. Auto-encoding variational bayes. *arXiv preprint arXiv:1312.6114*, 2013. 2, 4, 9
- [14] Black Forest Labs. Flux. <https://github.com/black-forest-labs/flux>, 2024. 12
- [15] Xingjian Leng, Jaskirat Singh, Yunzhong Hou, Zhenchang Xing, Saining Xie, and Liang Zheng. Repa-e: Unlocking vae for end-to-end tuning with latent diffusion transformers. *arXiv preprint arXiv:2504.10483*, 2025. 6
- [16] Tianhong Li, Yonglong Tian, He Li, Mingyang Deng, and Kaiming He. Autoregressive image generation without vector quantization. *Advances in Neural Information Processing Systems*, 37:56424–56445, 2024. 8
- [17] Yizhuo Li, Yuying Ge, Yixiao Ge, Ying Shan, and Ping Luo. Aligning latent spaces with flow priors. *arXiv preprint arXiv:2506.05240*, 2025. 2, 5
- [18] Yaron Lipman, Ricky TQ Chen, Heli Ben-Hamu, Maximilian Nickel, and Matt Le. Flow matching for generative modeling. *arXiv preprint arXiv:2210.02747*, 2022. 3
- [19] Nanye Ma, Mark Goldstein, Michael S Albergo, Nicholas M Boffi, Eric Vanden-Eijnden, and Saining Xie. Sit: Exploring flow and diffusion-based generative models with scalable interpolant transformers. In *European Conference on Computer Vision*, pages 23–40. Springer, 2024. 3, 8
- [20] Alireza Makhzani, Jonathon Shlens, Navdeep Jaitly, Ian Goodfellow, and Brendan Frey. Adversarial autoencoders. *arXiv preprint arXiv:1511.05644*, 2015. 3, 9

- [21] Maxime Oquab, Timothée Darcet, Théo Moutakanni, Huy Vo, Marc Szafraniec, Vasil Khalidov, Pierre Fernandez, Daniel Haziza, Francisco Massa, Alaaeldin El-Nouby, et al. Dinov2: Learning robust visual features without supervision. *arXiv preprint arXiv:2304.07193*, 2023. 1, 2, 6, 9
- [22] Ben Poole, Ajay Jain, Jonathan T Barron, and Ben Mildenhall. Dreamfusion: Text-to-3d using 2d diffusion. *arXiv preprint arXiv:2209.14988*, 2022. 3
- [23] Alec Radford, Jong Wook Kim, Chris Hallacy, Aditya Ramesh, Gabriel Goh, Sandhini Agarwal, Girish Sastry, Amanda Askell, Pamela Mishkin, Jack Clark, et al. Learning transferable visual models from natural language supervision. In *International conference on machine learning*, pages 8748–8763. PmLR, 2021. 9
- [24] Aditya Ramesh, Mikhail Pavlov, Gabriel Goh, Scott Gray, Chelsea Voss, Alec Radford, Mark Chen, and Ilya Sutskever. Zero-shot text-to-image generation. In *International conference on machine learning*, pages 8821–8831. Pmlr, 2021. 1
- [25] Aditya Ramesh, Prafulla Dhariwal, Alex Nichol, Casey Chu, and Mark Chen. Hierarchical text-conditional image generation with clip latents. *arXiv preprint arXiv:2204.06125*, 1(2):3, 2022. 1
- [26] Ali Razavi, Aäron van den Oord, Ben Poole, and Oriol Vinyals. Preventing posterior collapse with delta-vaes. *arXiv preprint arXiv:1901.03416*, 2019. 3, 9
- [27] Danilo Jimenez Rezende and Fabio Viola. Taming vaes. *arXiv preprint arXiv:1810.00597*, 2018. 3, 9
- [28] Robin Rombach, Andreas Blattmann, Dominik Lorenz, Patrick Esser, and Björn Ommer. High-resolution image synthesis with latent diffusion models. In *Proceedings of the IEEE/CVF conference on computer vision and pattern recognition*, pages 10684–10695, 2022. 1, 2, 3, 7, 9
- [29] Chitwan Saharia, William Chan, Saurabh Saxena, Lala Li, Jay Whang, Emily L Denton, Kamyar Ghasemipour, Raphael Gontijo Lopes, Burcu Karagol Ayan, Tim Salimans, et al. Photorealistic text-to-image diffusion models with deep language understanding. *Advances in neural information processing systems*, 35:36479–36494, 2022. 1
- [30] Minglei Shi, Haolin Wang, Wenzhao Zheng, Ziyang Yuan, Xiaoshi Wu, Xintao Wang, Pengfei Wan, Jie Zhou, and Jiwen Lu. Latent diffusion model without variational autoencoder. *arXiv preprint arXiv:2510.15301*, 2025. 1
- [31] Yang Song, Jascha Sohl-Dickstein, Diederik P Kingma, Abhishek Kumar, Stefano Ermon, and Ben Poole. Score-based generative modeling through stochastic differential equations. *arXiv preprint arXiv:2011.13456*, 2020. 1, 3, 5
- [32] Peize Sun, Yi Jiang, Shoufa Chen, Shilong Zhang, Bingyue Peng, Ping Luo, and Zehuan Yuan. Autoregressive model beats diffusion: Llama for scalable image generation. *arXiv preprint arXiv:2406.06525*, 2024. 8
- [33] Aaron Van Den Oord, Oriol Vinyals, et al. Neural discrete representation learning. *Advances in neural information processing systems*, 30, 2017. 1, 9
- [34] Zhengyi Wang, Cheng Lu, Yikai Wang, Fan Bao, Chongxuan Li, Hang Su, and Jun Zhu. Prolificdreamer: High-fidelity and diverse text-to-3d generation with variational score distillation. *Advances in neural information processing systems*, 36: 8406–8441, 2023. 9
- [35] Jingfeng Yao, Cheng Wang, Wenyu Liu, and Xinggang Wang. FASTERdit: Towards faster diffusion transformers training without architecture modification. *Advances in Neural Information Processing Systems*, 37:56166–56189, 2024. 8
- [36] Jingfeng Yao, Bin Yang, and Xinggang Wang. Reconstruction vs. generation: Taming optimization dilemma in latent diffusion models. In *Proceedings of the Computer Vision and Pattern Recognition Conference*, pages 15703–15712, 2025. 1, 2, 3, 4, 7, 8, 9, 12
- [37] Tianwei Yin, Michaël Gharbi, Taesung Park, Richard Zhang, Eli Shechtman, Fredo Durand, and Bill Freeman. Improved distribution matching distillation for fast image synthesis. *Advances in neural information processing systems*, 37:47455–47487, 2024. 9, 12
- [38] Tianwei Yin, Michaël Gharbi, Richard Zhang, Eli Shechtman, Fredo Durand, William T Freeman, and Taesung Park. One-step diffusion with distribution matching distillation. In *Proceedings of the IEEE/CVF conference on computer vision and pattern recognition*, pages 6613–6623, 2024. 2, 3, 4, 5, 9
- [39] Lijun Yu, José Lezama, Nitesh B Gundavarapu, Luca Versari, Kihyuk Sohn, David Minnen, Yong Cheng, Vighnesh Birodkar, Agrim Gupta, Xiuye Gu, et al. Language model beats diffusion–tokenizer is key to visual generation. *arXiv preprint arXiv:2310.05737*, 2023. 9
- [40] Xiaohua Zhai, Basil Mustafa, Alexander Kolesnikov, and Lucas Beyer. Sigmoid loss for language image pre-training. In *Proceedings of the IEEE/CVF international conference on computer vision*, pages 11975–11986, 2023. 2, 6, 9
- [41] Boyang Zheng, Nanye Ma, Shengbang Tong, and Saining Xie. Diffusion transformers with representation autoencoders. *arXiv preprint arXiv:2510.11690*, 2025. 1, 2, 4, 8, 9
- [42] Mingyuan Zhou, Huangjie Zheng, Zhendong Wang, Mingzhang Yin, and Hai Huang. Score identity distillation: Exponentially fast distillation of pretrained diffusion models for one-step generation. In *Forty-first International Conference on Machine Learning*, 2024. 9

Appendix

A. Implementation Details

Our methodology involves a multi-stage training pipeline. We detail the hyperparameters and architecture for each stage below.

A.1. Tokenizer Pretraining

We first train an initial AutoEncoder compressing the latents to a low dimension. We employ the pre-trained DINO-v2-large model (300M parameters) as our visual encoder. Given an input resolution of 256×256 , the encoder yields a 16×16 latent feature map. Following [3], we introduce an MLP projection head with a hidden dimension of 2048 to project the encoder features into a compact latent dimension of 32. For the decoder, we adopt a convolution-based architecture similar to Flux [14]. During this phase, we freeze the parameters of the DINO-v2 encoder and exclusively optimize the MLP projector and the decoder. The model is trained on the ImageNet dataset with a batch size of 256 and a learning rate of 1×10^{-4} for 8 epochs (40k steps).

We optimize the tokenizer using a composite objective function comprising reconstruction and adversarial terms. Following [4], the total loss L_{total} is:

$$L_{\text{total}} = L_1 + L_{\text{perceptual}} + \lambda_{\text{gan}} L_{\text{gan}} \quad (10)$$

where we set the adversarial weight $\lambda_{\text{gan}} = 0.5$.

A.2. Reference Distribution (Teacher) Pretraining

In this stage, we train a teacher model to capture the reference distribution. We first extract the latent representations for the entire ImageNet dataset using the frozen encoder and projector from the previous stage trained tokenizer. We then employ the LightningDiT-XL architecture with QKNorm (675M parameters) as our generative backbone to model these latents. This teacher model is trained to minimize the flow matching loss (Eq. 5). We follow the standard training recipe from VAAE[36], using a batch size of 1024, a learning rate of 2×10^{-4} , and train for 400 epochs (500K steps).

A.3. Distribution Matching VAE Training

This stage is the core of our method, where we jointly train the VAE and a student model to align the VAE’s latent space with the reference distribution. The framework involves three components: the AE (from Tokenizer pretraining stage), the teacher model (from reference pretraining stage) and the student model (initialized from teacher model).

We initialize the AE from the tokenizer pretraining stage checkpoint and the student model with the weights of the frozen teacher. The optimization is twofold:

- **VAE:** The VAE is updated by minimizing a composite objective: the reconstruction loss (Eq. 10) and the distribution matching (DM) loss (Eq. 9). The DM loss serves to align the VAE’s latent posterior with the reference distribution defined by the teacher.
- **Student Model:** The student (“fake”) model is simultaneously optimized to model the VAE’s evolving latent distribution by minimizing a score-based loss (Eq. 8).

We adopt a learning rate of 2×10^{-5} for both trainable models (the VAE and the student). The distribution matching loss term is scaled by a weight of $\lambda_{\text{dm}} = 10$, and we apply a classifier-free guidance (CFG) scale of $w = 5$ during the computation of the DM loss. Following the strategy in [37], we employ an alternating update schedule: the VAE is updated once every 5 iterations, while the student model is optimized at every training step. The joint training process is conducted for 350K steps.

A.4. Decoder Fine-tuning

Similar to [3], we fine-tune the decoder of the DM-VAE. We freeze the encoder and MLP projector, optimizing only the decoder with the reconstruction objective (Eq. 10). This fine-tuning is run for 250K steps, using a batch size of 256 and a learning rate of 1×10^{-4} .

A.5. Diffusion Model Training

After the DM-VAE is fully trained, we now train a final, high-fidelity generative model within its latent space. We train a new LightningDiT-XL model from scratch on DM-VAE latents, again optimizing for the flow matching loss (Eq. 5). This training is conducted with a batch size of 1024, a learning rate of 2×10^{-4} , and runs for 800 epochs (1M steps).

B. Visualization of DMD Gradient Direction

We visualize the DMD update vectors (i.e., the negative gradient field) using a 2D toy example in Figure 7. As observed, relying on a large noise scale leads to coarse and potentially inaccurate update directions. However, as discussed in Section 3.2, high noise levels are practically necessary to bridge the gap between distributions with initially disjoint supports. Conversely, a small noise scale yields highly precise update directions, but may fail to provide meaningful guidance when the distributions are far apart. The training process can be regarded as an averaging of different time steps, which demonstrates the value of dynamically adjusting the noise schedule during training. This needs further exploration.

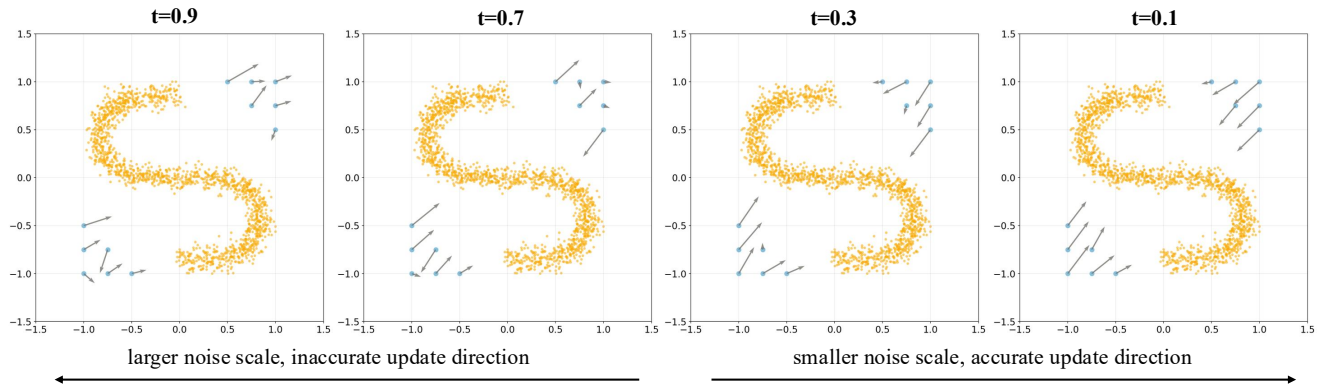
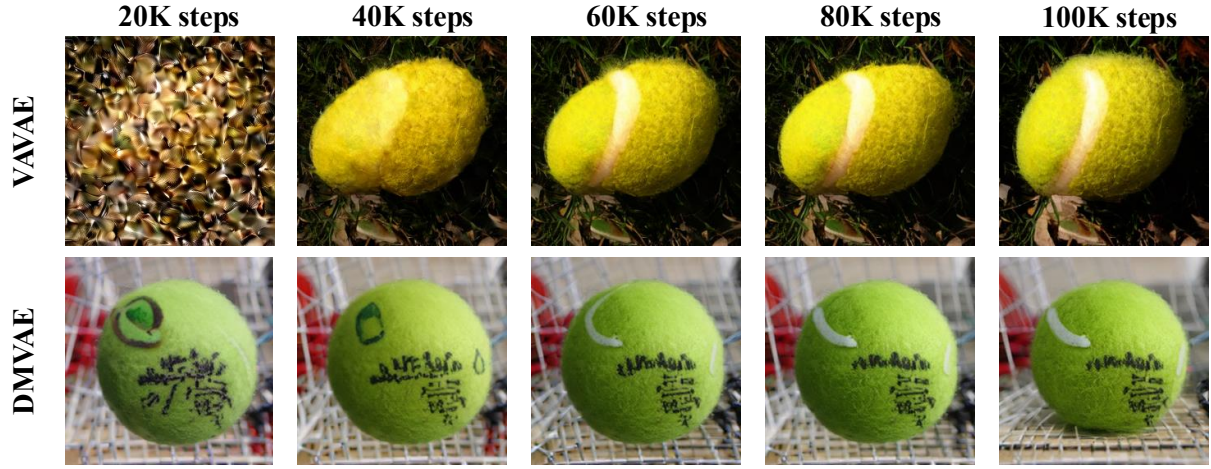


Figure 7. DMD update direction visualized at different timesteps in a 2D toy setting.

C. Convergence Speed Visualization

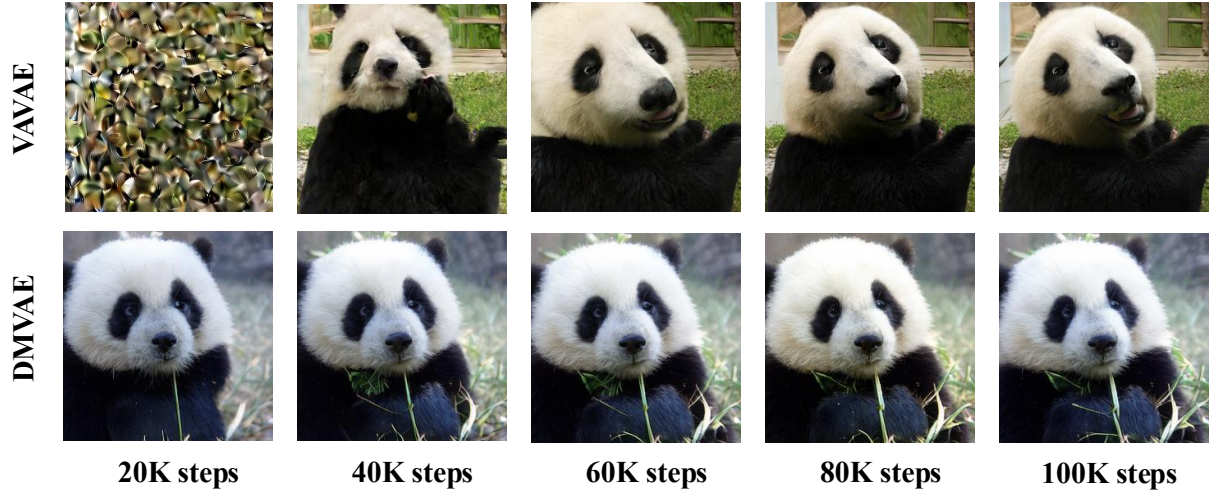
We present a visual comparison of the convergence speed between DMVAE and VAVAE in Figure 8. The results demonstrate that DMVAE achieves consistently superior visual generation quality compared to VAVAE when evaluated at equivalent training steps.



Class Name: “tennis ball”



Class Name: “macaw”



Class Name: “giant panda”

Figure 8. **Quantitative comparison of convergence speed on ImageNet 256×256 .** We compare DMVAE with VAAE and report conditional results without CFG.